Journal of Magnetic Resonance **139,** 273–280 (1999)
Article ID jmre.1999.1775, available online at http://www.idealibrary.com on IDEAL®

Measurement of Homonuclear ^2J-Couplings from Spin-State Selective Double-/Zero-Quantum Two-Dimensional NMR Spectra

Perttu Permi,*[,1] Sami Heikkinen,* Ilkka Kilpeläinen,* and Arto Annila†

*Institute of Biotechnology, University of Helsinki, P.O. Box 56, FIN-00014 Helsinki, Finland; and
†VTT Chemical Technology, P.O. Box 1401, FIN-02044 VTT Espoo, Finland

Received November 18, 1998; revised March 22, 1999

^{1}H-detected two-dimensional double-/zero-quantum experiments are described for measurement of homonuclear $^2J_{HH}$-couplings of NH_2 or CH_2 groups in proteins. These experiments utilize multiple-quantum coherence for determination of the size and the absolute sign of the geminal scalar and dipolar couplings in the presence of broad lines. Spectra are simplified by gradient selection and spin-state selective filters. © 1999 Academic Press

Key Words: **couplings; HB-GAM; multiple-quantum coherence; spin-state-selective filters; ubiquitin.**

INTRODUCTION

Measurement of scalar coupling constants has been of interest for years. Several techniques have been developed to determine, in particular, three-bond couplings which yield dihedral angle restraints for structure determination of macromolecules. For example, E.COSY (*1–4*) and quantitative *J*-correlation (*5–7*) methods are based on the evolution of small couplings during a defined period of time, whereas *J*-resolved experiments allow measurement of coupling constants, modulated during an incremented delay, directly from the in- or antiphase *J*-splitting (*8–10*). E.COSY provides also relative signs of coupling constants. Post-acquisitional methods such as *J*-deconvolution can be used to extract coupling constants from time or frequency domain data. Recently, it was shown that zero- and double-quantum spectroscopy also provides means to determine both signs and sizes of couplings (*11*) and more recently, the principle was refined for heteronuclear experiments (*12–14*).

Obviously, two-bond scalar couplings have not attracted much attention because there are no associated conformational degrees of freedom. However, introduction of residual dipolar couplings to high resolution NMR spectroscopy (*15–17*) calls for means to measure also ^2J-couplings in macromolecules. Dipolar coupling between geminal protons is comparable in strength to that between proton and nitrogen (or carbon). Proton–proton dipolar couplings of NH_2 (or CH_2) groups provide information on amino acid side chain orientation. The possibility of measuring dipolar couplings of three nonredundant internuclear vectors (H_1–H_2, H_1–N, and H_2–N) allows one to determine the orientation and to assess the dynamics of NH_2 (or CH_2) groups. The sign of the homonuclear scalar and dipolar couplings, which cannot be inferred simply from a conventional HSQC-*J* spectrum, is essential for the interpretation of spatial information. In general, the sign of a coupling is either obtained relative to a known coupling, or deduced from strong coupling effects. In this communication we describe a method based on double- and zero-quantum (DQ/ZQ) spectroscopy (*11–14*) for determining the sign and magnitude of the coupling between geminal protons. The methods presented are based on work originally presented by Jarvet and Allard (*14*). We have improved the basic pulse sequence for sensitivity and in addition have implemented spin-state selective filters (*18–20*) to the sequences to allow separation of multiple components into two subspectra. The α/β-half-filters used earlier in HSQC experiments (*18*) are modified for the present purpose to purge undesired components of transverse nitrogen magnetization. Furthermore, double- and zero-quantum spectra are separated into two additional subspectra by a pulsed field gradient selection. This double editing provides useful spectral simplification for studies of biomolecules.

DESCRIPTION OF THE PULSE SEQUENCES

The pulse sequences designed for the DQ/ZQ- and spin-state selective α/β-filtered DQ/ZQ correlation spectra are shown in Figs. 1A and B, respectively. The initial 90° proton pulse followed by a delay $(1/2J_{XH})$ and the nonselective 90° pulse for the heteronucleus generate a mixed double- and zero-quantum coherence (DQ/ZQ) between the proton and the heteronucleus. DQ evolves during t_1 with the sum of proton and heteronucleus chemical shifts while ZQ evolves with the difference of the chemical shifts. More importantly, DQ evolves during t_1 with the sum of the passive *J*-couplings, and ZQ evolves with the difference. Thus, NH_2 (or CH_2) cross peaks

[1] To whom correspondence should be addressed. Fax: +358-9-708 59541, E-mail: Perttu.Permi@helsinki.fi.

1090-7807/99 $30.00

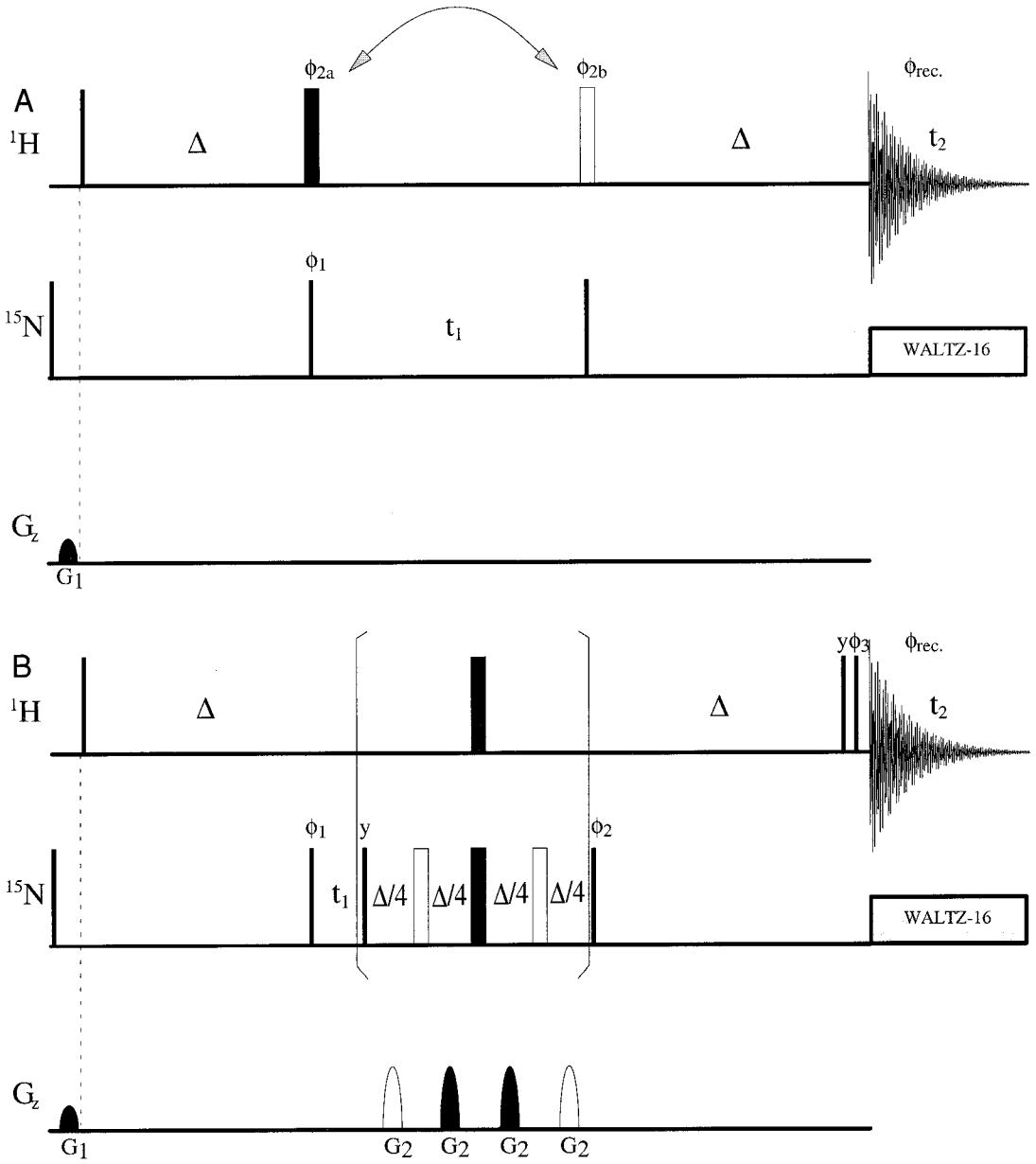

FIG. 1. Pulse sequences of the DQ/ZQ- (A) and α/β-half-filtered DQ/ZQ (B) experiments for determination of $^2J_{HH}$ coupling constants. Hard 90° and 180° pulses are indicated by narrow and wide bars, respectively, and are applied with the phase x, unless otherwise indicated. Delay durations: $\Delta = 1/4J_{XH}$. Phase cycling for the DQ/ZQ experiment (A): $\phi_1 = 8(x, -x)$; $\phi_{2a} = x, x, y, y, -x, -x, -y, -y$; $\phi_{2b} = x, x, y, y, -x, -x, -y, -y$; $\phi_{rec} = 4(-y, y, y, -y)$. Two data sets for each t_1 increment are collected to achieve quadrature in t_1. The 180° pulse on proton is applied simultaneously with the 90° pulse on nitrogen prior to the t_1 evolution period (ϕ_{2a}) for uneven multiples of eight transients (eight transients are needed to complete EXORCYCLE (*26*)) and simultaneously with the 90° pulse following the t_1 period (ϕ_{2b}) for even multiples of eight transients. From the first data set cosine modulated magnetization is extracted by addition of the FIDs. For the second data set, the FIDs are subtracted to give sine modulated magnetization ($\phi_{rec} = 2(-y, y, y, -y)$, $2(y, -y, -y, y)$). Phase cycling for the α/β-half-filtered DQ/ZQ experiment (B): $\phi_1 = 4(x, -x)$; $\phi_2 = 2(x, x, -x, -x)$ for the in-phase spectrum, $\phi_2 = 2(y, y, -y, -y)$ for the antiphase spectrum; $\phi_3 = 4(y)$, $4(-y)$; $\phi_{rec} = 2(-y, y, y, -y)$. Two data sets for each t_1 increment are collected to achieve quadrature in t_1. From the first data set, cosine modulated magnetization is extracted by addition of the FIDs. For the second data set, the FIDs are subtracted to give sine modulated magnetization. In the experiment (B), the 90° and 180° ^{15}N pulses denoted by (un)filled narrow and wide bars are applied for (in)- and antiphase α/β-half-filter elements. Gradient pulses denoted by unfilled half-ellipses are applied only during the in-phase α/β-half-filter element. A phase-sensitive spectrum is obtained by combining the data for Fourier transformation in a manner similar to the sensitivity-enchanced method (*21*, *22*). The absolute sign of geminal J- or dipolar coupling is obtained by relating $^2J_{HH}$ to the sign of $^1J_{NH}$ or $^1J_{CH}$. All magnetization originating from heteronucleus (^{15}N) is first dephased by the 90° pulse, followed by the pulsed field gradient.

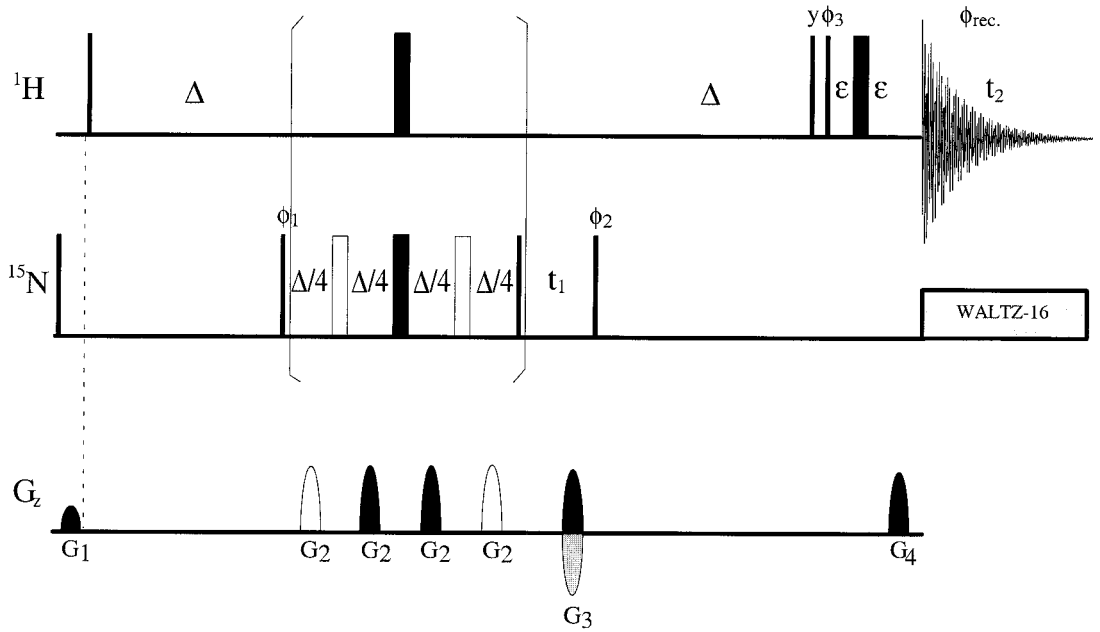

FIG. 2. Pulse sequence of the gradient selected α/β-half-filtered DQ/ZQ experiment. The sequences generate in- and antiphase spectra. Hard 90° and 180° pulses are shown by narrow and wide bars, respectively, with phase x, unless otherwise indicated. Delay durations: $\Delta = 1/4J_{XH}$ and ϵ is the duration of a pulsed field gradient including the field recovery delay. Phase cycling: $\phi_1 = 2(x, -x)$; $\phi_2 = 2(x)$, $2(-x)$ for the in-phase spectrum, $\phi_2 = 2(y)$, $2(-y)$ for the antiphase spectrum; $\phi_3 = 4(-y)$ for the echo selection; $\phi_3 = 4(y)$ for the anti-echo selection; $\phi_{rec} = x, -x, -x, x$. In addition to the echo/anti-echo selection, ϕ_1 is altered according to the States–TPPI protocol (*27*). A phase-sensitive spectrum is obtained by combining the data for Fourier transformation in a manner similar to the sensitivity-enchanced method (*21, 22*). Zero- and double-quantum coherences of ^{1}H and ^{15}N are separated into two subspectra by setting $G_3 = 0.908{*}G_4$ and $G_3 = 1.113{*}G_4$, respectively.

are modulated by both the large $^1J_{NH}$ (or $^1J_{CH}$) coupling and the small homonuclear coupling.

Spin-state selective filter elements in the experiment 1B (Fig. 1B) provide spectral simplification. An α/β-half-filter element subsequent to the evolution time, referred as antiphase α/β-half-filter, is used to rephase the sine modulated antiphase DQ/ZQ coherence with respect to the common passive spin. (In this case ^{15}N 180° pulses, indicated with unfilled bars, are not applied.) Another α/β-half-filter, referred as in-phase α/β-half-filter, is applied to select the cosine modulated in-phase magnetization component. (In this case 90° and 180° pulses on nitrogen, indicated as filled bars in the filter element, are not applied.) During the antiphase α/β-half-filter element, both homo- and heteronuclear couplings to the common passive spin are active, while heteronuclear coupling is effectively inactive during the in-phase α/β-half-filter element. Thus, the NH_2 cross peaks are anti- or in-phase doublets in the F_1-dimension in the antiphase or in-phase filter experiments, respectively. Regarding transverse relaxation and cross correlation between dipole–dipole coupling and chemical shift anisotropy (CSA), these two equally long filters are designed to guarantee the same sensitivity, which simplifies processing.

After the t_1 evolution and the filtering period in the α/β-filtered experiment, the antiphase single-quantum coherence is regenerated with the 90° pulse for the heteronucleus and is allowed to rephase during the final delay ($1/2J_{XH}$). In the experiment 1A two data sets for each t_1 increment are collected to achieve quadrature in t_1. For both data sets, a 180° proton pulse is applied before and after the t_1 evolution period (marked with an arrow in Fig. 1A; see Fig. 1 legends for details). In the case of the α/β-filtered experiment 1B this is achieved by applying two 90° proton pulses at the end of the pulse sequence with the same or opposite phase. This procedure retains both x- and y-components of magnetization and improvement in sensitivity by factor of $2^{1/2}$ (*14*). The post-acquisitional addition and subtraction of the two data sets result in quadrature detection in t_1.

Furthermore, zero- and double-quantum coherences can be separated into two subspectra for improved spectral resolution. This is conveniently accomplished by gradient selection in conjunction with the spin-state selective filters (Fig. 2). The phase of the last 90° proton pulse is shifted by 0° relative to the previous proton 90° pulse to select echo and by 180° to select anti-echo. The ratios of the selection (G_s) and refocusing (G_r) gradients for the heteronuclear double- and zero-quantum coherence selection are $G_s/G_r = \pm\gamma_H/(\gamma_H + \gamma_X)$ and $G_s/G_r = \pm\gamma_H/(\gamma_H - \gamma_X)$, respectively, where γ_H and γ_X denote proton and heteronuclear magnetogyric ratios (*14*). Thus, for the ^{15}N-edited spectrum, the selection gradient is 1.113 times stronger than the refocusing gradient for the double-quantum coherence

selection, and for the zero-quantum coherence pathway, the corresponding ratio is 0.908. The α/β-half-filter element is placed before the t_1 evolution in the gradient-selected version; otherwise the 90° purge pulse on nitrogen would mix the coherence levels during t_1, leading to unsuccessful selection between the double- and zero-quantum coherences. We prefer to apply the selection gradient at the beginning of the t_1 evolution period. Obviously, the first few data points are lost because the sum of the gradient duration and field recovery delay is longer than a few dwell times. However, the first few data points can be recovered by linear prediction to avoid baseline roll due to chemical shift evolution. Alternatively, the selection gradient can be applied in an $\epsilon/4$–180(^{1}H)–$\epsilon/4$–180(^{15}N)–$\epsilon/4$–180(^{1}H)–$\epsilon/4$ element to prevent evolution of the chemical shift and coupling between ^{1}H and ^{15}N. Data acquired with the gradient-selected version are processed identically to the data processed by established PEP sensitivity-enhanced gradient methods (*21, 22*) to achieve the same sensitivity as that obtained with the phase-modulated, phase-cycled version. In summary, the processing of the spin-state, DQ/ZQ selective acquisition will result in four subspectra.

The water signal can be suppressed in both phase-cycled and gradient-selected versions by selective pulses and pulsed field gradients prior to the actual pulse sequences, e.g., by the WET solvent suppression scheme (*23*).

The coherence transfer pathway in α/β-filtered experiments for the H_1H_2N (or H_1H_2C) system (neglecting signs, certain trigonometric factors, and homonuclear J-modulation during three delays optimized for $1/2J_{NH}$) is:

$$H_{1z} \xrightarrow{90^\circ_x(^1\mathrm{H})-1/2J-90^\circ_x(^{15}\mathrm{N})} H_{1x}N_y.$$

Mixed DQ/ZQ coherence evolves during t_1 with passive couplings to H_2. Only desired magnetization components are shown, i.e., for one filter sine modulated and for the other cosine modulated chemical shift and J-coupling in the t_1-dimension.

$$H_{1x}N_y \xrightarrow{t_1} H_{1x}N_y\cos((\Omega_{H_1} \pm \Omega_N)t_1) \times \cos((J_{H_1-H_2} \pm J_{N-H_2})\pi t_1)$$

$$+ H_{1x}H_{2z}N_y\sin((\Omega_{H_1} \pm \Omega_N)t_1) \times \sin((J_{H_1-H_2} \pm J_{N-H_2})\pi t_1).$$

The sine modulated magnetization evolves from the antiphase DQ/ZQ coherence to the in-phase coherence during the antiphase α/β-half-filter element:

$$H_{1x}H_{2z}N_y\sin((\Omega_{H_1} \pm \Omega_N)t_1)\sin((J_{H_1-H_2} \pm J_{N-H_2})\pi t_1) \xrightarrow{90^\circ_y(^{15}\mathrm{N})-1/4J-180^\circ_x(^1\mathrm{H},\,^{15}\mathrm{N})-1/4J} H_{1x}N_x\sin((\Omega_{H_1} \pm \Omega_N)t_1)\sin((J_{H_1-H_2} \pm J_{N-H_2})\pi t_1).$$

The 90° pulse on nitrogen serves to purge ^{15}N magnetization terms with phase x. Therefore, a dispersive in-phase term arising from $^1J_{NH}$-mismatch will not convert into observable magnetization. After the filter period, the desired sine modulated magnetization is converted back to detectable magnetization by a 90° pulse on the heteronucleus. Then the antiphase magnetization evolves back to an in-phase y-magnetization, which is detected during t_2 under heteronuclear broadband decoupling:

$$H_{1x}N_x\sin((\Omega_{H_1} \pm \Omega_N)t_1) \times \sin((J_{H_1-H_2} \pm J_{N-H_2})\pi t_1) \xrightarrow{90^\circ_y(^{15}\mathrm{N})-1/2J} H_{1y}\sin((\Omega_{H_1} \pm \Omega_N)t_1)\sin((J_{H_1-H_2} \pm J_{N-H_2})\pi t_1).$$

Heteronuclear J-coupling is inactive during the in-phase α/β-half-filter element. Thus, the cosine modulated magnetization does not evolve and is converted back to proton single-quantum coherence by a 90° pulse on nitrogen. For the in-phase α/β-half-filter experiment, the phase of the last 90° pulse on nitrogen is incremented by 90° relative to the antiphase α/β-half-filtered experiment:

$$H_{1x}N_y\cos((\Omega_{H_1} \pm \Omega_N)t_1)\cos((J_{H_1-H_2} \pm J_{N-H_2})\pi t_1) \xrightarrow{1/8J-180^\circ_x(^{15}\mathrm{N})-1/8J-180^\circ_x(^1\mathrm{H})-1/8J-180^\circ_x(^{15}\mathrm{N})-1/8J} H_{1x}N_y\cos((\Omega_{H_1} \pm \Omega_N)t_1)\cos((J_{H_1-H_2} \pm J_{N-H_2})\pi t_1) \xrightarrow{90^\circ_x(^{15}\mathrm{N})-1/2J} H_{1y}\cos((\Omega_{H_1} \pm \Omega_N)t_1)\cos((J_{H_1-H_2} \pm J_{N-H_2})\pi t_1).$$

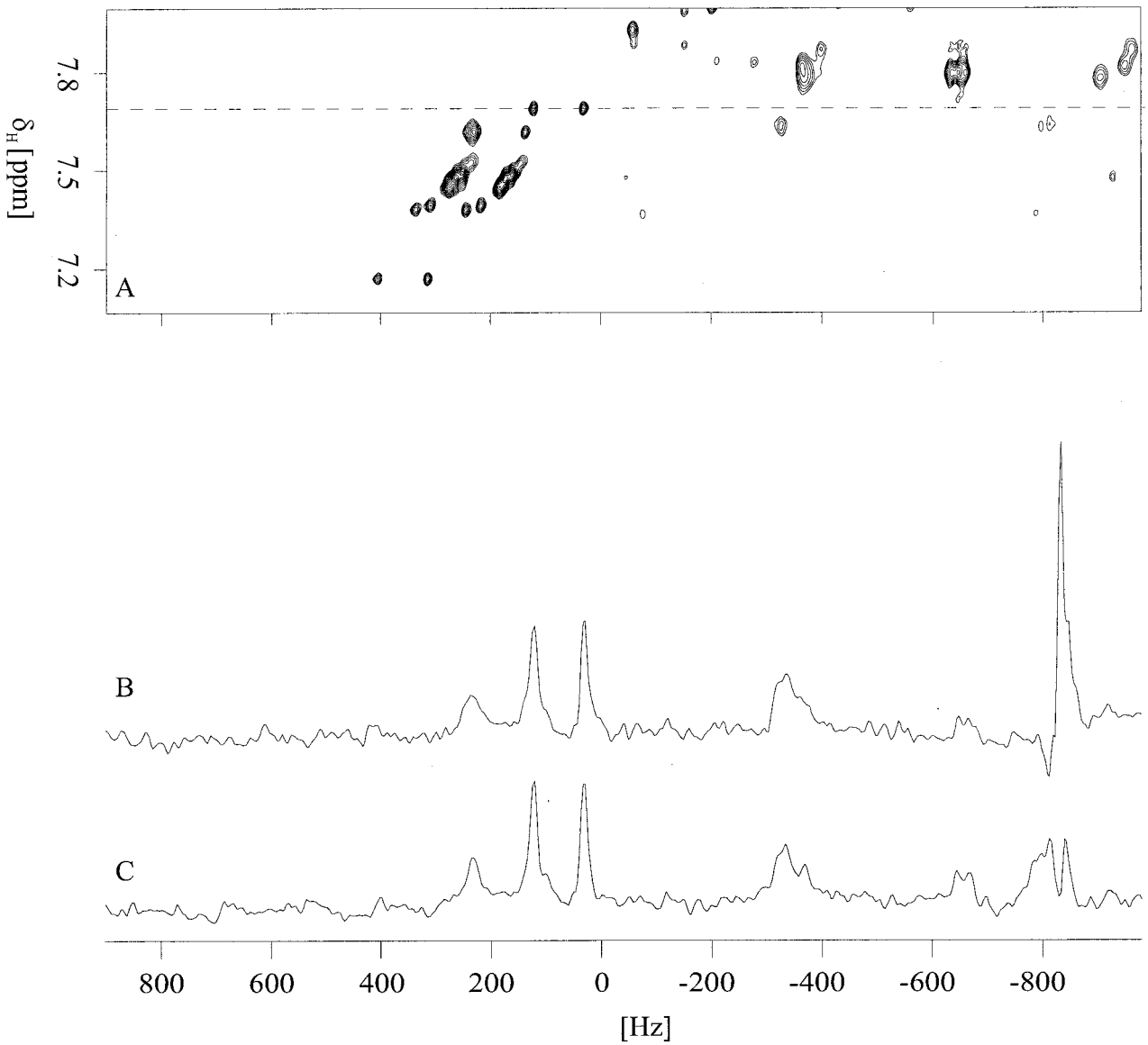

FIG. 3. Representative ZQ region of the HB-GAM ^{15}N, ^{1}H DQ/ZQ spectrum recorded with the pulse sequence shown in Fig. 1A (A). The dashed line identifies the location of the cross section shown in (C). A corresponding cross section through the ZQ region of a combined DQ/ZQ spectrum recorded with the original pulse sequence is shown in (B) (*14*). Experimental parameters: 1.1 m*M* ^{15}N-enriched HB-GAM in 95/5% H_2O/D_2O, pH 4.7, in a Shigemi microcell. All spectra were recorded on a Varian Unity 500 spectrometer at 30°C. Delay durations: $\Delta = 2.77$ ms, $\epsilon = 0.952$ ms. Gradient amplitude (duration): $|G_1| =$ 5.3 G/cm (1000 μs). Spectral widths in the F_1-dimension (F_2-dimension): 3500 (8000) Hz. The ^{1}H carrier on water resonance was at 4.7 ppm; number of t_1 increments, 400; acquisition time (t_2), 128 ms. The signal at -800 Hz originates in water, which was suppressed by the WET scheme (*23*). Data were zero-filled to 2K in the F_1-dimension. The FID was apodized in the F_2-dimension using an exponential window function with 10 Hz line broadening. A squared cosine window function was applied to the F_1-dimension. Data were processed with the Felix97.0 software package (*28*).

This allows upfield and downfield doublet components to be separated into two subspectra by adding or subtracting the sine modulated absorptive antiphase and cosine modulated absorptive in-phase magnetizations.

In all experiments, undesired dispersive antiphase magnetization arising from homonuclear *J*-modulation during t_1 evolves and is converted into term $H_{1x}H_{2z}$ after refocusing. Usually this term cancels from the spectrum due to a relatively small homonuclear coupling compared with broad linewidths and apodization in the F_2-dimension by the exponential window function (*9*). Effects of homonuclear ^{13}C–^{13}C *J*-coupling must be considered for ^{13}C-labeled samples. Carbonyl decoupling during t_1 for the CH_2 group of glycines in ^{13}C-edited experiments will easily suffice to remove the ^{13}C–^{13}C modulation. For other amino acids, modulation of the homonuclear ^{13}C–^{13}C coupling is not as easily removed during t_1 and the α/β-half-filtering period. Furthermore, the active proton is coupled to these passive carbon spin(s) by $^2J_{CH}$. Therefore, a

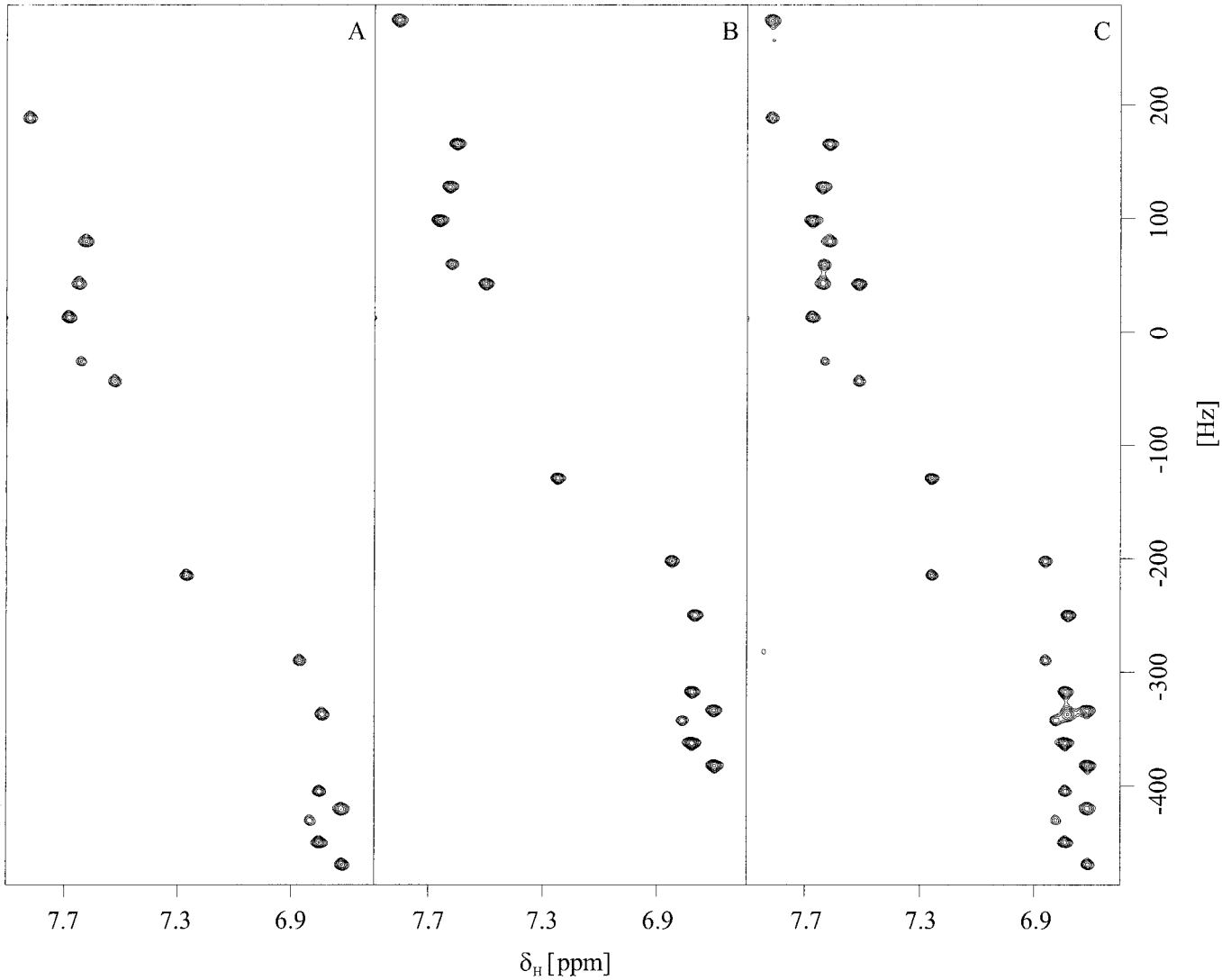

FIG. 4. Representative DQ region of the ubiquitin α/β-half-filtered ^{15}N, ^{1}H DQ/ZQ spectrum recorded with the pulse sequence shown in Fig. 1B. Addition and subtraction of the in- and antiphase components from two experiments result in up- (A) and downfield (B) components, respectively. For reference, the DQ region from the DQ/ZQ spectrum (C) is shown, containing both spin states in-phase. Sample conditions: 1.0 m*M* ubiquitin from VLI Research Inc. in 90/10% H_2O/D_2O, pH 5.8, 50 m*M* sodium phosphate buffer, in a Wilmad NMR tube. All spectra were recorded on a Varian Unity 500 spectrometer at 30°C. Delay durations: $\Delta = 2.77$ ms. Gradient amplitudes (durations): $|G_{1,2}| = 5.3$ G/cm (1000 μs), 30 G/cm (500 μs). Spectral widths in the F_1-dimension (F_2-dimension): 3500 (8000) Hz; number of t_1 increments, 600; acquisition time (t_2), 128 ms. The WET scheme was used for water suppression. Data were zero-filled to 4K in the F_1- and F_2-dimensions, resulting in a digital resolution of 0.85 Hz/Pt in the F_1-dimension. The FID was apodized in the F_2-dimension using exponential window function with 15 Hz line broadening. A squared cosine window function was applied in the F_1-dimension.

DQ- or ZQ-doublet is further split into a doublet of doublets (triplet) each of which is modulated by $^{1}J_{CC} \pm {}^{2}J_{CH}$, resulting in a broad and complicated peak pattern.

RESULTS AND DISCUSSION

The pulse sequences presented were demonstrated with two proteins: 15 kDa ^{15}N-enriched heparin-binding growth-associated molecule (HB-GAM) (*24*) and 8.6 kDa ^{15}N-enriched human ubiquitin. A combined DQ/ZQ spectrum was recorded for HB-GAM with the pulse sequence shown in Fig. 1A. A representative expansion of the ZQ spectral region of the combined DQ/ZQ spectrum containing cross peaks of NH_2 resonances is shown in Fig. 3A. The dashed line in the spectrum indicates the location of the cross section shown in Fig. 3C. Figure 3B provides a comparison for the cross sections from a spectrum recorded with the pulse sequence proposed by Jarvet and Allard (*14*). In our hands, after careful adjustment of ^{1}H and ^{15}N pulse widths, the overall signal-to-noise ratio (*S*/*N*) was improved by 10–15%, using the pulse sequence presented in Fig. 1A. This small gain in *S*/*N* results

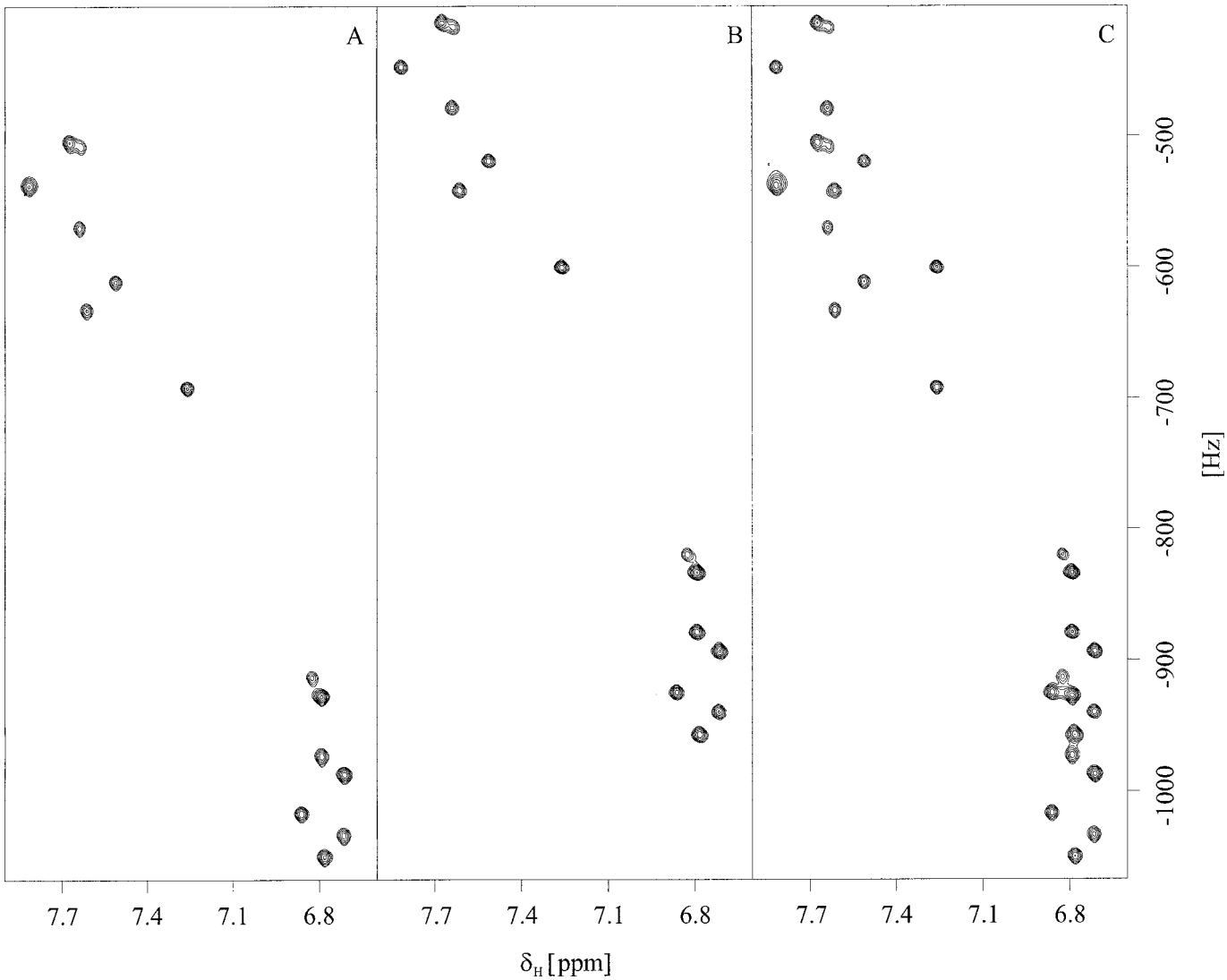

FIG. 5. Representative ZQ region of the ubiquitin α/β-half-filtered ^{15}N, ^1H ZQ spectrum recorded with the pulse sequence shown in Fig. 2. Addition and subtraction of the in- and antiphase components from two experiments result in up- (A) and downfield (B) components, respectively. The ZQ spectrum (C) is shown for reference, containing both of the spin states in-phase. Experimental parameters were the same as those for the spectrum shown in Fig. 4, except for the gradient strengths (durations) $|G_{1,2,3,4}|$ = 5.3 G/cm (1000 μs), 30 G/cm (500 μs), 10.896 G/cm (500 μs), 12 G/cm (500 μs), and delay ϵ = 0.952 ms. Additionally, backward linear prediction was used to reconstruct the first three data points to give a flat baseline.

from fewer pulses. The actual improvement in performance will depend on RF field inhomogeneity and off-resonance effects.

The spin-state selective, combined DQ/ZQ spectra were recorded for ubiquitin with the pulse sequence shown in Fig. 1B. Double- and zero-quantum coherences were also separated into two subspectra by recording the spectra with the pulse sequence shown in Fig. 2. Expansions of the ZQ spectral region of the combined DQ/ZQ spectrum containing cross peaks of NH_2 resonances are shown in Fig. 4. Figures 4A and 4B show the ZQ region with up- (A) and downfield (B) components of doublets, respectively. These were obtained by adding and subtracting the in- and antiphase spectra. The ZQ cross peaks are split in the F_1-dimension by the sum of the $^1J_{N-H_2}$ and $^2J_{H_1-H_2}$ couplings. Figure 4C is used as reference and shows both upfield and downfield in-phase doublet components, acquired with the pulse sequence 1B, using the in-phase α/β-half-filter.

The corresponding DQ resonances from the gradient selected DQ spectrum with the upfield (A) and downfield (B) components are shown in Fig. 5. Figure 5C is used for reference and shows both of the DQ doublet components, obtained by the pulse sequence using the in-phase α/β-half-filter. DQ cross peaks are split by the difference of the couplings $^1J_{N-H_2}$ and $^2J_{H_1-H_2}$. The geminal $^2J_{H_1-H_2}$ coupling constant can be determined using the equation

TABLE 1
Measured Geminal $^2J_{HH}$ Coupling Constants from Human Ubiquitin

Residue	$^2J_{HH}$ (Hz)	
	H_{21}	H_{22}
Gln2	3.0	3.1
Asn25	2.1	2.2
Gln31	2.6	2.5
Gln40	2.8	2.7
Gln41	3.6	3.7
Gln49	3.0	3.1
Asn60	2.9	3.1
Asn62	3.1	3.1

$$\frac{J_{DQ} - J_{ZQ}}{2} = {}^2J_{HH}, \qquad [1]$$

where J_{DQ} and J_{ZQ} denote double- and zero-quantum splittings in the F_1-dimension, respectively. Analogously, $^1J_{N-H_1}$ and $^1J_{N-H_2}$ couplings can be determined using the equation

$$\frac{J_{DQ} + J_{ZQ}}{2} = {}^1J_{NH}. \qquad [2]$$

The sign can be inferred by comparing J_{DQ} with J_{ZQ}. Residual proton–proton dipolar contributions to the coupling can be determined in an analogous way once the scalar coupling is known from a reference experiment. Geminal $^2J_{H_1-H_2}$ coupling constants determined for the eight asparagine and glutamine residues of human ubiquitin are shown in Table 1.

The experiments presented are not sensitive to dipole–dipole and CSA cross correlation, because inversion of proton spin states in both α/β-half-filter elements averages relaxation rates for DQ/ZQ doublet components. The current method also reduces effects arising from scalar relaxation of the second kind (*25*). Thus, the apparent coupling constant is not significantly affected by line broadening due to rapid spin flips of protons, which in most cases reduce the value of experimentally determined coupling constants. As the effect of the scalar relaxation of the second kind to $^2J_{HH}$ is inversely proportional to the magnitude of DQ/ZQ splittings, the current method is not sensitive to this phenomenon (*12*).

In conclusion, we have introduced spin-state selective, double- vs zero-quantum experiments. These methods allow a convenient extraction of geminal proton–proton couplings arising from scalar or dipolar interactions. Our results imply that the methods are suitable also for measuring other two-bond couplings, in particular from isotopically enriched macromolecules. The scalar and dipolar couplings which are easy to assign provide dihedral and orientational restraints to significantly complement NOE-based distance restraints for the structure determination.

ACKNOWLEDGMENTS

The authors thank Professors Gottfried Otting and Poul Erik Hansen for valuable and helpful discussions. This work was supported by the Academy of Finland.

REFERENCES

1. C. Griesinger, O. W. Sørensen, and R. R. Ernst, *J. Am. Chem. Soc.* **107,** 6394 (1985).
2. C. Griesinger, O. W. Sørensen, and R. R. Ernst, *J. Chem. Phys.* **85,** 6837 (1986).
3. P. Phändler and G. Bodenhausen, *J. Magn. Reson.* **72,** 475 (1987).
4. G. T. Montelione, M. E. Winkler, P. Rauenbuehler, and G. Wagner, *J. Magn. Reson.* **82,** 198 (1989).
5. A. Bax, D. Max, and D. Zax, *J. Am. Chem. Soc.* **114,** 6923 (1992).
6. B. Reif, M. Köck, R. Kerssebaum, J. Schleucher, and C. Griesinger, *J. Magn. Reson. B* **112,** 295 (1996).
7. J. S. Hu and A. Bax, *J. Am. Chem. Soc.* **119,** 6360 (1997).
8. D. Neuhaus, G. Wagner, M. Vasak, J. H. R. Kägi, and K. Wüthrich, *Eur. J. Biochem.* **151,** 257 (1985).
9. L. E. Kay and A. Bax, *J. Magn. Reson.* **86,** 110 (1990).
10. S. Heikkinen, H. Aitio, P. Permi, R. Folmer, K. Lappalainen, and I. Kilpeläinen, *J. Magn. Reson.* **137,** 243 (1999).
11. L. Braunschweiler, G. Bodenhausen, and R. R. Ernst, *Mol. Phys.* **48,** 535 (1983).
12. A. Rexroth, P. Schmidt, S. Szalma, T. Geppert, H. Schwalbe, and C. Griesinger, *J. Am. Chem. Soc.* **117,** 10389 (1995).
13. G. Otting, *J. Magn. Reson.* **124,** 503 (1997).
14. J. Jarvet and P. Allard, *J. Magn. Reson. B* **112,** 240 (1996).
15. A. Bax and N. Tjandra, *J. Biomol. NMR* **10,** 289 (1997).
16. J. R. Tolman, J. M. Flanagan, M. A. Kennedy, and J. H. Prestegard, *Proc. Natl. Acad. Sci. U.S.A.* **92,** 9279 (1995).
17. N. Tjandra and A. Bax, *J. Magn. Reson.* **124,** 512 (1997).
18. P. Andersson, J. Weigelt, and G. Otting, *J. Biomol. NMR* **12,** 435 (1998).
19. A. Meissner, J. Ø. Duus, and O. W. Sørensen, *J. Biomol. NMR* **10,** 89 (1997).
20. A. Meissner, J. Ø. Duus, and O. W. Sørensen, *J. Magn. Reson.* **128,** 92 (1997).
21. A. G. Palmer III, J. Cavanagh, P. E. Wright, and M. Rance, *J. Magn. Reson.* **93,** 151 (1991).
22. L. E. Kay, P. Kiefer, and T. Saarinen, *J. Am. Chem. Soc.* **114,** 10663 (1992).
23. S. H. Smallcombe, S. L. Patt, and P. A. Kiefer, *J. Magn. Reson. A* **117,** 295 (1995).
24. H. Rauvala and P. Peng, *Prog. Neurobiol.* **52,** 127 (1997).
25. A. Abragam, "Principles of Nuclear Magnetism," Clarendon Press, Oxford (1961).
26. G. Bodenhausen, R. Freeman, and D. L. Turner, *J. Magn. Reson.* **27,** 511 (1977).
27. D. Marion, M. Ikura, R. Tschudin, and A. Bax, *J. Magn. Reson.* **85,** 393 (1989).
28. FELIX 97.0, Biosym/MSI, San Diego, 1997.